https://doi.org/10.5194/egusphere-2026-3046
Preprint. Discussion started: 28 July 2026

Development of an automated contrail-to-flight attribution using Meteosat Second Generation satellite data

Sabrina Ries[1], Luca Bugliaro[2], Vanessa Santos Gabriel[1], Dennis Piontek[2], Matteo Aricò[1,2], and Christiane Voigt[1,2]

[1]Institute of Atmospheric Physics, Johannes Gutenberg University, Mainz, Germany
[2]Deutsches Zentrum für Luft- und Raumfahrt, Institut für Physik der Atmosphäre, Oberpfaffenhofen, Germany

Correspondence: Sabrina Ries (sries@uni-mainz.de)

Abstract. Persistent contrails are a major contributor to the effective radiative forcing from aviation. Optimizing flight trajectories to avoid regions prone to the formation of warming contrails has therefore been proposed as a mitigation strategy to achieve the international climate targets for the aviation sector. However, the precise attribution of observed contrails to individual flights remains a challenge for both the evaluation of avoidance measures and the validation of contrail models. This study presents a fully automated evaluation framework designed for matching contrails to flights using observations from the Spinning Enhanced Visible and Infra-Red Imager (SEVIRI) instrument aboard the geostationary Meteosat Second Generation (MSG) satellite and flight trajectories. The method utilizes an automated contrail detection algorithm. Although such automated detections designed for MSG/SEVIRI often face a trade-off between high detection efficiency and low false alarm rate, the proposed matching process substantially improves detection reliability through a multi-step verification: contrails are preselected based on their spatial and temporal occurrence as well as their spatial orientation with respect to the flight trajectories, followed by temporal tracking. A new aspect is the development of a life cycle-based confidence score to derive a quantitative matching score. In contrast to previous approaches, the proposed method is entirely observation-driven, requires no model input, and enables rapid, large-scale application. The framework's performance is demonstrated through two specific case studies. Future applications include the assessment of contrail avoidance trials across the Europe-African airspace and adaptation to other satellite configurations.

1 Introduction

Contrails (condensation trails) are narrow, linear ice-clouds that form in the cold upper troposphere from aircraft engine emissions (Voigt et al., 2026). Under ice-supersaturated conditions, contrails can persist for hours (Vázquez-Navarro et al., 2015), spread with wind shear, dissipate or subsequently evolve into contrail cirrus. While persistent contrails represent only a fraction of all contrails (Teoh et al., 2022a, 2024), they have a net warming effect (Meerkötter et al., 1999; Myhre and Stordal, 2001; Burkhardt and Kärcher, 2011), which dominates aviation's non-CO_2 radiative forcing (Lee et al., 2021). Given the resumed increase in global air traffic after the COVID crisis, the radiative forcing associated with contrails is expected to further increase in future (Schumann et al., 2021; Gettelman et al., 2021).

https://doi.org/10.5194/egusphere-2026-3046
Preprint. Discussion started: 28 July 2026

In the context of international climate targets – such as achieving climate-neutral aviation by 2050 (ATAG, 2021) – the need to mitigate the short-lived non-CO_2 effects of aviation has gained increasing importance. Different measures address these effects including the use of alternative fuels, such as sustainable aviation fuels (Voigt et al., 2021; Teoh et al., 2022b; Märkl et al., 2024) or hydrogen (Bier et al., 2024; Lottermoser and Unterstrasser, 2025, 2026), cleaner burning engines (Voigt et al., 2026) and climate-optimized flight routing (Mannstein et al., 2005; Grewe et al., 2017; Teoh et al., 2020a, b; Martin Frias et al., 2024). To implement such re-routing strategies, forecasts of temperature and ice-supersaturated regions (ISSR) are utilized to adjust flight paths either in advance or during flight to avoid persistent contrail formation (Teoh et al., 2020a). These strategies often rely on models like the Contrail Cirrus Prediction (CoCiP) model (Schumann, 2012), which estimate contrail formation, evolution, and radiative forcing. However, significant challenges remain, including operational constraints such as delays and flight level occupancy, forecast stability (Dean et al., 2025; Bonhorst et al., 2025), as well as inherent uncertainties in contrail and weather models. In particular, some weather models have a limited accuracy in their prediction of ice-supersaturation (e.g. Gierens et al., 2020). Implementing contrail avoidance measures may involve a trade-off, potentially leading to slightly increased CO_2 emissions due to longer flight trajectories (Martin Frias et al., 2024; Kirschler et al., 2026). To investigate the risks or benefits of contrail avoidance, Prather et al. (2025) developed a risk-assessment framework demonstrating that CO_2 increases are likely offset by non-CO_2 reductions at trade-off ratios as high as 1:5. Applying this framework, Voigt (2025) highlighted the high probability for a net climate benefit for fleet-wide contrail avoidance strategies (Martin Frias et al., 2024). Progressing a step beyond, Smith et al. (2026) calculated the climate damage for late implementation of contrail avoidance measures, which is estimated to be substantial.

Despite these challenges, first real-world implementation trials have been conducted and evaluated (e.g. Sausen et al., 2024; Sonabend-W et al., 2024; Kirschler et al., 2026). However, verifying the success of such trials remains a major challenge. Model-based assessments of the climate impact mitigation potential of the demonstration trials are required, but are subject to many uncertainties, including e.g. simplified contrail model parametrizations and inaccuracies in the underlying numerical weather prediction data. Observation-based evaluation methods vary depending on the trial design: while some trials aim to clear entire sectors of air traffic, negating the need for individual contrail-to-flight matching (Sausen et al., 2024), others reroute single flights, which necessitates a direct attribution of observed contrails to specific aircraft (Sonabend-W et al., 2024; Kirschler et al., 2026). A primary difficulty in this individual matching is the observational time gap between contrail formation and its detection in satellite imagery. As described by Vázquez-Navarro et al. (2015), this gap–defined largely by the imager's spatial resolution and meteorology–can lead to a significant advection-caused displacement between the flight trajectory and the observed contrail. To bridge this observational spatio-temporal gap, flight trajectories are in previous studies advected using numerical wind data for spatial comparison with contrails detected in geostationary satellite imagery. These advection-based approaches have primarily been developed for the US domain using data from the American Geostationary Operational Environmental Satellite (GOES) and its Advanced Baseline Imager (ABI). However, initial efforts relied on manual evaluation to match advected trajectories with observed contrails (Sonabend-W et al., 2024), which is subjective, time-consuming and therefore their application is limited. Consequently, recent developments have moved toward automated matching algorithms. For instance, Chevallier et al. (2023) developed a framework that integrates deep learning-based instance segmentation, trajectory

https://doi.org/10.5194/egusphere-2026-3046
Preprint. Discussion started: 28 July 2026

advection using NWP wind fields, and aircraft matching into a single process. Gryspeerdt et al. (2024) attributed contrails to the closest advected flight path. Similarly, Geraedts et al. (2024) optimized a cost function for the agreement between advected flight path and observed contrails based on the relative distance and the age of the advected trajectories to identify the most likely generating aircraft. However, wind-advection methods suffer from two sources of uncertainty that significantly degrade attribution accuracy and increase false-positive rates. First, the horizontal advection relies on NWP or reanalysis wind fields, which carry inherent uncertainties of 2–6 $\mathrm{m\,s^{-1}}$ (7.2–21.6 $\mathrm{km\,h^{-1}}$) in wind speed and mean absolute wind direction differences of more than $50°$ compared to observations (Schumann et al., 2013; Geraedts et al., 2024; Wu et al., 2024). Over typical advection periods of 1–2 h, this wind error accumulates to a substantial horizontal trajectory displacement of up to several tens of kilometres. Second, persistent contrails undergo wake-vortex sinking, sedimentation, and vertical shear, extending over several hundred meters in height. Given that strong vertical wind shear in the tropopause region can reach $0.02\,\mathrm{s^{-1}}$ ($= 20\,\mathrm{m\,s^{-1}\,km^{-1}}$) (Kaluza et al., 2021), even a vertical offset of only a few hundred metres can translate into several metres per second of horizontal wind error. If this vertical displacement is neglected or incorrectly modelled—due to NWP temperature and ice-supersaturation biases or simplified microphysics—trajectory advection accesses wind vectors at the wrong altitude, further amplifying horizontal drift errors. A further problem for all such methods remains the lack of external reference data (i.e., "ground truth"). To address this, Sarna et al. (2025) introduced a synthetic model-based reference dataset for GOES to test and validate the performance of attribution algorithms.

The reliable attribution of contrails to their generating aircraft is essential not only for verifying avoidance trials but also for the evaluation of contrail models. In this study, we present a new automated approach designed to process large datasets. A key distinction of our algorithm is its independence from external wind data; instead, it determines contrail advection by tracking them within satellite observations. By eliminating reliance on weather models, we directly circumvent the two primary sources of uncertainty outlined above: the inherent inaccuracies in modelled wind fields and the altitude-dependent advection errors caused by contrail settling. Specifically developed for the European Meteosat Second Generation (MSG) satellite/Spinning Enhanced Visible and Infra-Red Imager (SEVIRI) sensor, this method provides a robust framework for assessing the contrail-to-flight attribution by tracking contrails in consecutive satellite images and applying a set of spatio-temporal and geometric criteria. For this purpose, high temporal resolution Rapid Scan data from MSG/SEVIRI are used. Sect. 2 presents the tools used for observation-based contrail-to-flight matching. Subsequently, Sect. 3 presents the key steps of the contrail-to-flight matching method, which first involves the collocation of the satellite and flight data (Sect. 3.1), followed by contrail selection based on geometric criteria (Sect. 3.2), yielding contrails that lie in close spatio-temporal proximity to the flight trajectory and exhibit a similar orientation. This is followed by a two-step contrail tracking procedure to reconstruct the observable contrail life cycle (Sect. 3.3). Subsequently, the requirements for a consistent contrail-to-flight match are defined (Sect. 3.4), providing the basis for a quantitative assessment of the spatio-temporal agreement between aircraft trajectories and observed contrail life cycles (Sect. 3.5). Finally, the proposed method is applied to example flights (Sect. 3.6). In a sensitivity analysis (Sect. 4), the method is evaluated with respect to the influence of contrail detection and matching parameters. An application to the real-world flight trial conducted over Germany in 2024 (e.g. Kirschler et al., 2026) is presented in a companion paper.

https://doi.org/10.5194/egusphere-2026-3046
Preprint. Discussion started: 28 July 2026

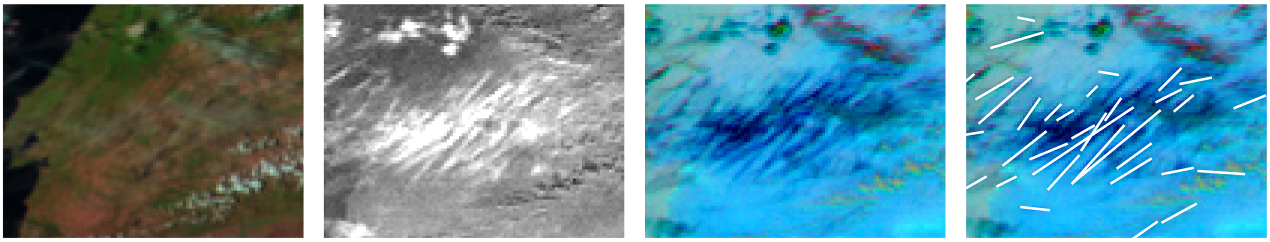

(a) (b) (c) (d)

Figure 1. Comparison of different channel combinations from the MSG/SEVIRI acquired on 01 October 2016 at 15:00 UTC. All images show the same region of Spain and Portugal with contrails: (a) Natural RGB image, (b) 10.8-12.0 μm BTD image with a scale from -1 to 6 K and (c) Ash RGB image, (d) Ash RGB image with contrail detections overlaid using the COCOS algorithm (Santos Gabriel et al., 2026b).

2 Methods

2.1 Contrail Remote Sensing with Meteosat Second Generation

Continuous monitoring of contrails over Europe requires observations at day and night with high temporal resolution. To meet these requirements, this study uses data from the geostationary Meteosat Second Generation (MSG) satellites (Schmetz et al., 2002). The main geostationary satellite of the MSG series, located at 0° E, provides uninterrupted coverage of Europe as well as of the Middle East, Africa, and parts of the Atlantic Ocean. Each of the four geostationary satellites (MSG1 to MSG4) is equipped with the Spinning Enhanced Visible and Infra-Red Imager (SEVIRI) radiometer, which acquires images of the Earth in twelve spectral channels (four in the solar spectrum and eight in the infrared spectrum) every 15 min with a spatial resolution of 3 km $\times$ 3 km at the sub-satellite point, increasing to approximately 6 km $\times$ 3 km over Central Europe (EUMETSAT, 2024) due to the Earth's curvature and the larger viewing angle. One of the MSG satellites, positioned at 9.5° E, provides a Rapid Scan Service that focuses on the northern third of the SEVIRI disk covering Europe. While the spatial resolution remains unchanged, the smaller coverage area allows the temporal resolution to be improved to 5 min; these Rapid Scan data from MSG4 are used in this study.

For contrail remote sensing, brightness temperature differences (BTDs) between the SEVIRI infrared channels at 10.8 μm and 12.0 μm and between 10.8 μm and 8.7 μm are particularly relevant as they show large values for thin ice clouds with small effective particle sizes and thus allow the identification of contrails (see e.g. Mayer et al., 2024). Furthermore the Ash RGB composite, which is a combination of the three infrared channels mentioned above, is also used to highlight contrails (e.g. Ng et al., 2024; EUMeTrain, 2022). Contrails are especially visible in the BTD image (Fig. 1b) as white lines and in the Ash RGB (Fig. 1c) as dark blue lines. Since only infrared channels are used, they are independent of daytime. However, the observation of contrails in MSG/SEVIRI satellite images is complicated. Key challenges are the geometric and optical characteristics of the contrails, the accuracy of the detection algorithm and the moderate spatial resolution of SEVIRI compared to the Advanced

https://doi.org/10.5194/egusphere-2026-3046
Preprint. Discussion started: 28 July 2026

Baseline Imager (ABI) aboard the Geostationary Operational Environmental Satellite (GOES) series, the Advanced Himawari Imager (AHI) on Himawari-8/9, and the Flexible Combined Imager (FCI) aboard the Meteosat Third Generation (MTG) satellites. Furthermore the visibility of contrails in the satellite imagery is affected by the prevailing meteorological conditions, especially the presence of thick ice clouds. In the following, we describe how these challenges are addressed in this study and which tools are developed and employed.

2.2 Contrail Detectability in MSG

Immediately after formation, contrails are narrow and therefore not visible in MSG/SEVIRI due to the larger size of the MSG pixels. With time, persistent contrails can broaden through diffusion and wind shear and are advected by atmospheric winds, appearing in satellite data displaced from the flight track, which is a key challenge for satellite-based contrail-to-flight matching. As the ice water path increases sufficiently, they become visible (Driver et al., 2025). Geraedts et al. (2024) show that contrails can already be detected as early as 20 min after formation over the US with the geostationary GOES/ABI satellite (Schmit et al., 2017), which has a higher spatial resolution of 2 km at the sub-satellite point compared to MSG/SEVIRI. In contrast, studies focusing on the coarser resolution of MSG/SEVIRI at mid-latitudes assume longer durations. Gierens and Vazquez-Navarro (2018) estimate a mean lifetime of 1.5 ± 0.4 h before a contrail expands sufficiently to fill a pixel and becomes visible. Variations in estimated first detection times result from variable meteorological conditions, such as ice supersaturation and wind shear, different viewing angles and instrument characteristics. The impact of these environmental factors is reflected in the varying reported/assumed contrail spreading rates, which range from 5 km h^{-1} (Gierens and Vazquez-Navarro, 2018) to a lower value of 2.7 km h^{-1} (Duda et al., 2004). Furthermore, contrails do not need to fill an entire pixel homogeneously to become visible; consequently, the actual time until first detection can be shorter than the duration required for full pixel coverage. In Sect. 3, we assume that contrails become visible in MSG/SEVIRI no earlier than 20 min and no later than 120 min after formation. Earlier appearance is highly unlikely, whereas later appearance remains possible but introduces increasing uncertainties in the contrail-to-flight matching process.

2.3 Contrail Detection with COCOS

The contrail detection algorithm COCOS (Santos Gabriel et al., 2026b) has been developed to identify line-shaped contrails. COCOS assigns a confidence score indicating detection certainty to each contrail. The choice of the confidence threshold is a trade-off between high detection efficiency and low false alarm rate. With the optimal confidence score of 0.465, the algorithm achieves a recall of 63.5 %, which measures the fraction of true contrails correctly identified, indicating that a large proportion of true contrails are successfully detected. Undetected contrails tend to be thin, shorter, occur over land, and are embedded in thin or thick ice clouds. At the same time, the algorithm exhibits relatively low precision of 14.5 %, which indicates the fraction of detected contrails that are actually real, meaning that it produces a high false alarm rate. The sensitivity of the matching results to the large number of false positives in contrail detection is analysed in Sect. 4.
COCOS identifies all contrail pixels and determines its endpoints, which are defined as the pair of pixels within the contrail object that are farthest apart from each other (Fig. 1d). The endpoints are used to parametrise the contrail as a line segment

https://doi.org/10.5194/egusphere-2026-3046
Preprint. Discussion started: 28 July 2026

with a given orientation and length. The contrail orientation is defined as the angle, in degrees, between the contrail line and the horizontal image axis of the MSG/SEVIRI grid, based on the contrail endpoints. Although this orientation depends on the considered part of the satellite disk, this approach is valid for this study as we only compare orientations of contrails and flight sections in close spatial proximity.

2.4 Contrail Visibility in the Presence of Cirrus Clouds

The visibility of contrails strongly depends on the presence of ambient cirrus clouds. In particular, for flights passing through, just above or below thick cirrus clouds, observability is limited (Ng et al., 2024), as the contrail signal is superimposed and attenuated by the ice clouds. Seelig et al. (2025) investigated the additional contribution to radiative forcing from young (< 30 min) contrails embedded in cirrus using lidar observations from satellite and they found a measurable effect (Wang and Voigt, 2025). Such dense cirrus layers can extend over several hundred kilometres, restricting contrail detection along large portions of the flight path and preventing a conclusive assessment of contrail formation. To account for these visibility limitations, cirrus cloud properties are derived using the CiPS (Cirrus Properties from SEVIRI) algorithm (Strandgren et al., 2017). It relies on a set of artificial neural networks trained with SEVIRI thermal observations, CALIOP (Cloud-Aerosol Lidar with Orthogonal Polarization (Winker et al., 2009)) backscatter measurements, ECMWF surface temperature data, and auxiliary information. CiPS identifies ice clouds and retrieves microphysical and geometrical properties, including cirrus cloud probability (CCP), cirrus opacity probability (COP, indicating whether the CALIOP backscatter signal was fully attenuated), cloud top height, ice optical thickness and ice water path. Detecting cirrus using a CCP threshold of 0.62, CiPS yields a probability of detection (POD) of 71 % and a false alarm rate (FAR) of 3.9 % when compared to 4.9 million CALIOP observations. To quantitatively account for this uncertainty, we determine the fraction of the trajectory located within or directly above thick ice clouds for each flight (details in Sect. 3.2). Thick ice clouds are defined in the following as pixels that contain opaque clouds (COP threshold of 0.86) or with an ice optical thickness larger than the empirical threshold 1.5, as Strandgren et al. (2017) indicate that nearly all clouds are opaque above this value..

2.5 Contrail Tracking with ACTA

Contrail tracking enables the analysis of the visible life cycle of contrails, allowing to estimate the time and location of contrail formation through backward extrapolation as well as their advection direction and speed. This information is crucial for associating observed contrails with individual flights as it allows us to bridge the time gap between first appearance in the satellite observations and the transit of the aircraft. For this study, the Automated Contrail Tracking Algorithm (ACTA) (Vazquez-Navarro et al., 2010) is used. As part of this work, the algorithm was translated from IDL to Python and partially modified and improved. A summary of the algorithm's functionality and the implemented modifications are provided in Appendix A. ACTA is capable of tracking older and non-linear segments, enabling to capture the full observable life cycle of contrails until their linearity is completely lost. The effectiveness of this approach for characterizing the temporal evolution and geometric properties of contrails has been demonstrated in previous statistical life-cycle studies (Vázquez-Navarro et al., 2015). In contrast, the COCOS detection algorithm does not establish temporal connections between detections at different times. Nevertheless,

https://doi.org/10.5194/egusphere-2026-3046
Preprint. Discussion started: 28 July 2026

the detection of a contrail at a given time is required to initiate the tracking process. Therefore, both methods – detection and tracking – are essential to represent the visible contrail life cycle as comprehensively as possible.

3 Contrail-to-Flight Matching

In this section, we present a multi-step method to automatically determine whether observed contrails are produced by a particular flight, providing a quantitative assessment of contrail-to-flight correspondence. The algorithmic workflow is schematically illustrated in Fig. 2. First, the aircraft trajectory is collocated with the satellite imagery in space and time and divided into 5 min sections (blue box) according to the MSG/SEVIRI Rapid Scan repetition rate. Contrail detection with COCOS is performed from departure up to 2 h after landing to capture contrails that appear with a delay along the full flight track. Detected contrails are initially filtered based on their position and orientation relative to the flight (yellow box). In the central analysis step, contrail tracking determines their temporal evolution through clustering and ACTA (green box). If the contrail life cycle is assessable, a matching score is calculated (orange box), which enables a quantitative derivation of the degree to which an observed contrail can be associated with the respective flight. The following sections describe each step in detail.

3.1 Collocation of Flight Trajectories with Satellite Images

In the first step, the aircraft trajectory is collocated with the 5 min Rapid Scan data to link contrails with the corresponding flight. Flight waypoints are mapped onto the SEVIRI grid, accounting for parallax caused by the viewing angle of the geostationary satellite and the aircraft's altitude. The flight points are then assigned to the nearest satellite image acquisition time. Since SEVIRI scans the Earth line by line over several minutes from South to North, multiple flight points fall within the same satellite image, dividing the trajectory into 5 min sections. Non-linear flight sections and altitudes below 7000 m are excluded, as the former cannot be identified by COCOS and the latter fall outside the typical range for persistent contrails formation (Petzold et al., 2020; Li et al., 2023).

3.2 Contrail Selection and Ice Clouds

Since contrails are not immediately visible in MSG/SEVIRI after their formation, each flight section is evaluated within a time window of 20 to 120 min after the aircraft has passed, corresponding to 21 satellite images at 5 min intervals. At each time step, detected contrails are tested against two criteria to determine whether they could have been produced in this flight section. Between formation and first detection, contrails can only be advected by the wind over a limited distance, and their orientation can only change within certain bounds. To account for horizontal advection, a maximum wind speed of $v_{\max} = 50\,\mathrm{km\,h^{-1}}$ at flight altitude is assumed. As actual mean wind speeds over Europe are generally lower (Simmons, 2022), this approach aims to capture all relevant contrails. Since wind direction is unknown, an oval-shaped region (called "shell" in the following) is defined with "radius" $\Delta t \cdot v_{\max}$ from the flight section (Fig. 3), where Δt is the elapsed time between the flight passage and contrail detection. We defined a position criterion stating that at least one of the contrail endpoints lies within this shell. Using SEVIRI's spatial resolution at the sub-satellite point, the shell expands at 1.39 pixels per 5 min. At the same time, to account

https://doi.org/10.5194/egusphere-2026-3046
Preprint. Discussion started: 28 July 2026

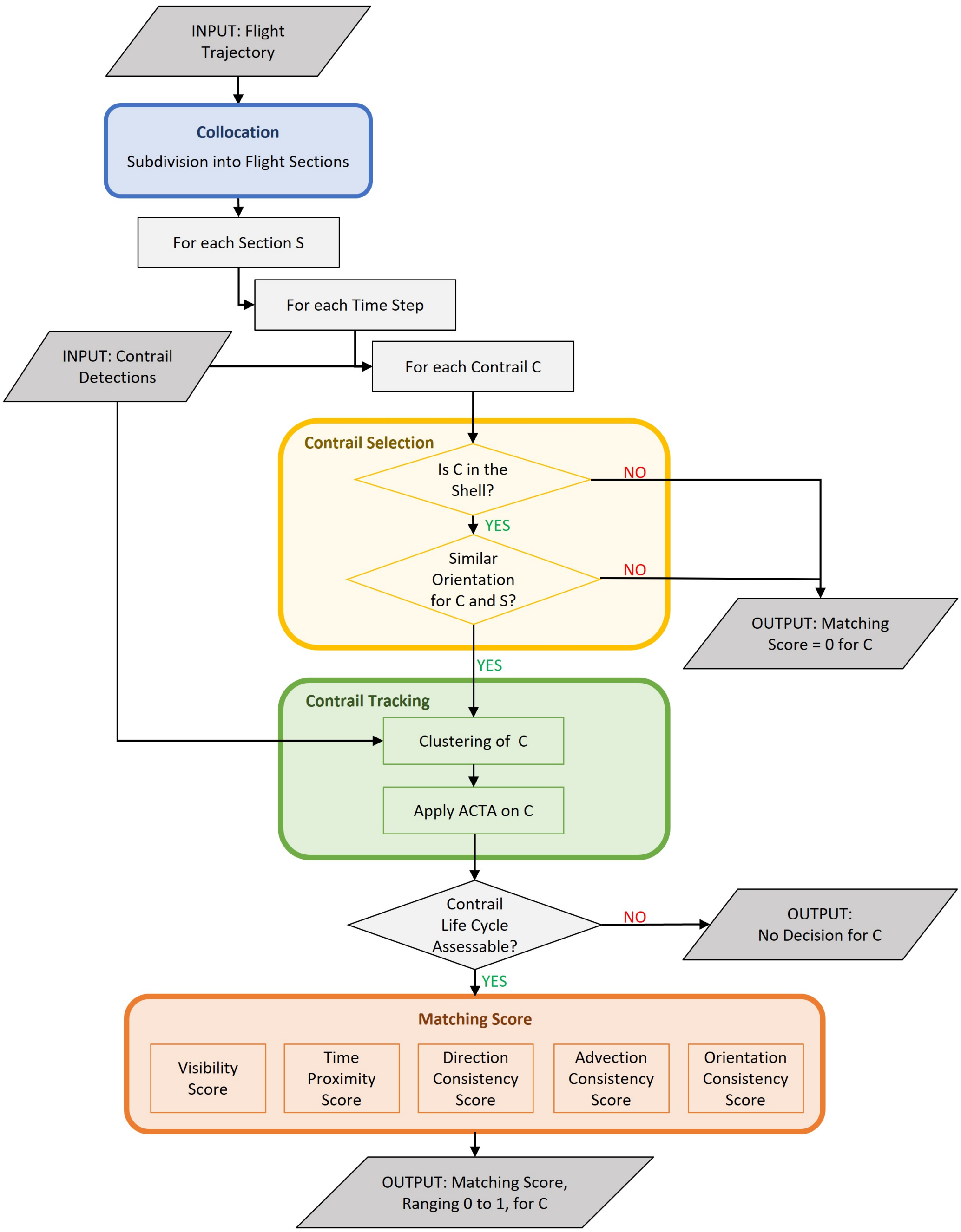

Figure 2. Schematic of the contrail-to-flight matching algorithm.

https://doi.org/10.5194/egusphere-2026-3046
Preprint. Discussion started: 28 July 2026

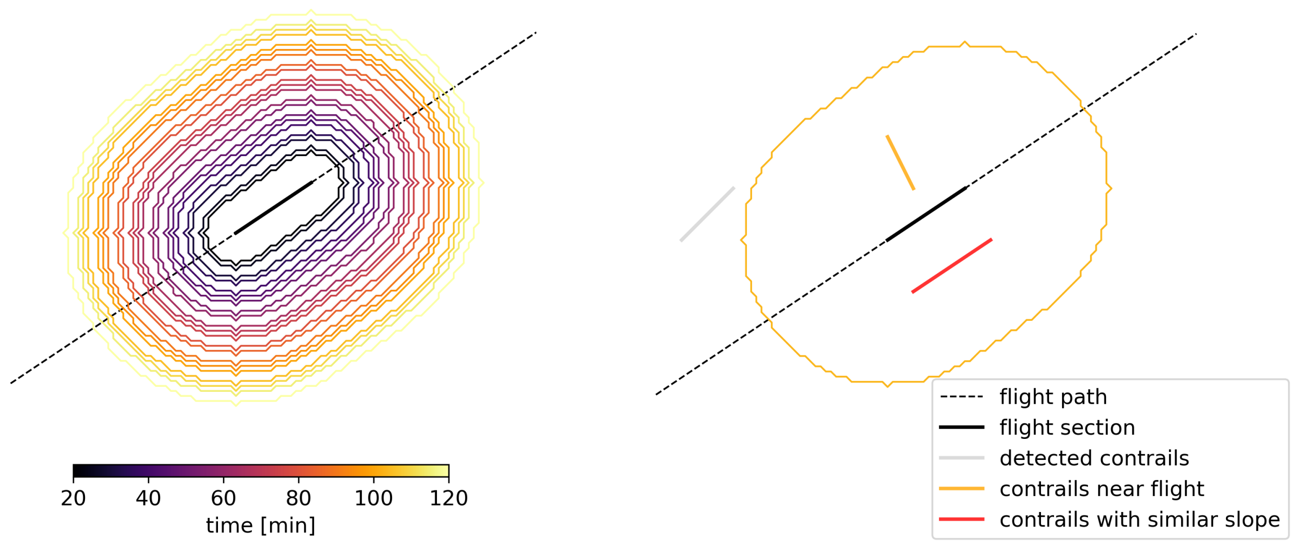

Figure 3. Illustration of the contrail selection criteria. Left: Flight section with the expanding shell at 5 min intervals, indicating the region where contrails could be located after advection from the flight section where they should have formed. Right: Flight section with detected contrails and the corresponding shell. Only contrails inside the shell and with similar orientation to the flight trajectory are considered for matching.

for limited contrail visibility in regions with thick ice clouds, the thick ice cloud cover (Sect. 2.4) is determined within the 21 shells.

Afterwards, the orientation of the contrails – defined as the orientation of the line connecting their endpoints – is compared to that of the flight section. Following Vazquez-Navarro et al. (2010), it is assumed that the orientation of a contrail can change by a maximum of 2.8° within 5 min due to horizontal wind shear. The contrails that do not fulfil both position and orientation criteria are assigned a matching score of zero and are not considered further. We call all contrails which fulfil these two criteria potential matches with the flight. Fig. 3 illustrates an example: although two of the three detected contrails lie within the shell, only the one highlighted in red meets both criteria. The orange contrail is excluded because it only satisfies the position criterion but fails the orientation requirement.

3.3 Contrail Life Cycle

In this step, the contrail life cycle is analysed by means of a contrail tracking procedure. Clustering is the initial part of contrail tracking and is designed to group (cluster) contrails in consecutive satellite images that correspond to the same physical contrail. Clustering proceeds as follows. Since contrail position, orientation, and length typically change little within a 5 min interval, contrails from adjacent time steps are grouped based on geometric criteria. A contrail near the one of interest with similar orientation and length is assumed to be the same physical contrail and assigned to the cluster. Three criteria are required

https://doi.org/10.5194/egusphere-2026-3046
Preprint. Discussion started: 28 July 2026

for two contrails in two consecutive images to belong to the same cluster: a) both endpoints lie within a 6-pixel shell (≈ 18 km at the sub-satellite point) of the starting contrail, b) orientation differs by no more than 0.2 rad (≈ 11.5°) and c) length ranges within 70 % to 130 % of the original. The choice for the values is explained in the next paragraph. Clustering starts with a random contrail at a given time and searches for contiguous contrails in previous or next time steps that satisfy the criteria. When a contrail is added, the search recursively extends to adjacent time steps. Additional contrails detected by COCOS that meet the clustering criteria may also be included, even if they initially fail selection criteria. This occurs, for example, if a contrail becomes visible earlier than 20 min after aircraft passage or appears closer to the trajectory later.

The clustering parameters are derived from empirical investigations, with a specific focus on accounting for detection uncertainties. These uncertainties have a disproportionately large impact during the clustering stage, which operates strictly on 5 min intervals. For instance, if the endpoints of a contrail are seven pixels apart, a displacement of a single endpoint by just one pixel can alter its orientation by approximately 8°. If the same tolerance used in the selection step (2.8° per 5 min) was applied here, such inherent geometric uncertainties could not be sufficiently absorbed. This tight constraint is appropriate for the selection step because that stage considers much larger time intervals of 20–120 min. Over such periods, the tolerance effectively scales to a range of 11.2°–67.2°, providing a larger buffer for alignment. In contrast, the 5 min clustering steps require a higher relative tolerance to maintain tracking stability. Consequently, the orientation tolerances are set larger than those in Sect. 3.2, and the search shell is expanded relative to Sect. 3.2 to accommodate potential increases in observable contrail length. The length tolerance assumes that the contrail remains a single contiguous structure. While this assumption may not always hold – for example, if a contrail splits – the subsequent application of the ACTA is designed to compensate for such fragmentation.

This computationally efficient clustering captures part of the contrail life cycle. It is complemented by ACTA, which tracks less linear or weakly detectable contrails, particularly during early formation stages when they are not yet or partially detected, or towards the end of the life cycle. ACTA requires an initial contrail and autonomously searches for temporally adjacent contrails. To reduce computational cost, it is applied only to the first and last detected contrail in each cluster, tracking them backward and forward in time, respectively. This circumvents the need to track every contrail individually, since clustering already identifies which detections belong to the same physical contrail. ACTA increases the number of contrails per cluster, providing a more complete representation of the contrail life cycle without changing the total number of clusters. By reconstructing a larger portion of the contrail life cycle, more precise information on location and time of formation, movement direction and speed is obtained. For example, the young contrails, which might be missed by clustering alone, may lie outside the allowed time window, and clusters with few contrail detections yield less reliable motion estimates. Once the clusters are finalized through clustering and ACTA, the spatio-temporal evolution of each contrail cluster is characterized. This includes deriving parameters such as the spatio-temporal origin determined by the intersection of the cluster axis and flight path, the cluster advection velocity, and the advection-derived contrail formation time. A description of the derivation of these parameters, along with a comprehensive uncertainty, is provided in the Appendix B.

In the following, consistency of the temporal evolution of the clustered contrails with the given flight track is quantified. First of all, we require that 1) a cluster contains at least two contrails and 2) the distance between the earliest and latest contrail positions exceeds 3 pixels such that quantities like advection velocity are not dominated by detection uncertainties or the lim-

https://doi.org/10.5194/egusphere-2026-3046
Preprint. Discussion started: 28 July 2026

ited spatial resolution, providing sufficient spatial variation for a meaningful assessment of advection, and avoiding unreliable results from closely spaced contrails. All contrail clusters that do not satisfy these requirements are assigned the status "no decision" because the temporal evolution of the contrails during their (early) life cycle cannot be assessed. This situation occurs predominantly for the large number of false alarms and is examined in detail in Sect. 4. In contrast, all contrail clusters satisfying these criteria are further evaluated in the next section.

3.4 Matching Criteria

Different aspects of the contrail life cycle are evaluated on a normalized scale from 0 (no association) to 1 (perfect match) according to the following five scores for all the clusters left (see end of previous section). Please note that for all of them the temporal evolution-related quantities can be determined. The specific thresholds and assigned values for all scores are summarized in Tab. C1.

The **Visibility Score** M_1 quantifies how well the potential contrail life cycle can be observed. It is based on the assumption that true contrails are typically visible over multiple consecutive time steps in MSG/SEVIRI Rapid Scan mode. The score depends on the number of consecutive detections, corresponding to the number of contrails in the cluster. The score increases linearly with the number of consecutive observations: it is 0.5 for two contrails, 0.75 for three, and reaches its maximum of 1.0 for four or more consecutive time steps. The lower bound of 0.5 ensures that the matching score described in Sect. 3.5 is not dominated by the number of detections alone, as a contrail may be physically consistent with the target flights even if it is only observed in a few time steps. The **Time Proximity Score** M_2 quantifies the temporal consistency between a cluster and a flight. As contrails become visible in satellite imagery only with a delay, the time of first visibility is compared to the estimated flight time of contrail formation.

Based on the expected appearance times of contrails in MSG/SEVIRI images discussed in Sect. 2.2, we define a scoring function for the temporal offset. While contrails may generally become visible between 20 and 120 min, higher probability for a reliable match typically falls within a core interval of 30 to 90 min. Consequently, the score M_2 is set to 1 for this interval, representing the highest confidence in the temporal alignment. For deviations towards the outer bounds (20 min and 120 min), the score decreases linearly to account for the increasing uncertainty at these extremes. Outside the 20 to 120 min window, M_2 is set to 0, as the contrail appears either too early or too late to be considered valid with respect to the flight.

The **Direction Consistency Score** M_3 quantifies whether after formation, contrails are advected away from their assumed point of origin due to upper-tropospheric winds ($M_3 = 1$) or not ($M_3 = 0$). The **Advection Consistency Score** M_4 compares the time difference Δt between advection-derived contrail formation time and actual flight time at contrail formation. Due to the uncertainties in the determination of the advection-derived contrail formation time and the underlying assumptions, we set $M_4 = 1$ when $\Delta t < 30$ min and let the score linearly decrease as Δt increases. For $\Delta t \geq 60$ min, we set $M_4 = 0$. The scores M_2 and M_4 address distinct physical uncertainties and provide independent information. M_2 focuses exclusively on the temporal delay between flight passage and the first contrail detection due to the spatial resolution of MSG/SEVIRI. In contrast, M_4 evaluates the spatial and kinematic alignment of the detected contrail. It assesses whether the contrail's observed position and its calculated advection speed are consistent with the flight path.

https://doi.org/10.5194/egusphere-2026-3046
Preprint. Discussion started: 28 July 2026

While individual contrail orientations are evaluated during the selection step, the **Orientation Consistency Score** M_5 assesses changes in contrail orientation within a cluster relative to the flight trajectory. The average angular velocities during the visible (ω_{visible}) and non-visible ($\omega_{\text{non visible}}$) periods are calculated as detailed in Tab. C1. The angular velocity in the non-visible period is determined using the flight trajectory orientation at formation (Θ_0) and the orientation of the first visible contrail (Θ_1) to approximate the start and end of the non-visible period, respectively. Θ_2 denotes the orientation of the last visible contrail, and $\Delta t_{\text{non visible}}$ and $\Delta t_{\text{visible}}$ are the corresponding time intervals in minutes. The closer the angular velocities of the two periods, the more consistent the contrail's orientation evolution with the flight trajectory. This assumes that the wind speed and direction remain constant throughout the contrail lifetime. The score is computed as a decaying exponential (Tab. C1) with scaling factor $\epsilon = 0.4\,°$/min, determined empirically to account for orientation uncertainties. An exponential decay function is chosen for M_5 to provide higher sensitivity to small angular deviations while maintaining a non-zero probability for larger variations.

3.5 Matching Score

The **matching score** M combines the five individual scores M_1 to M_5 and is computed as the penalized mean of them, yielding a number between 0 and 1:

$$M = 1.25 \cdot M_{\text{mean}} \cdot \frac{M_{\text{min}}}{0.25 + M_{\text{min}}}.$$

M_{mean} is the standard arithmetic mean of the scores, and M_{min} represents the minimum score value. The formula applies a penalty to the mean based on the minimum value: if M_{min} is small, the ratio $\frac{M_{\text{min}}}{0.25+M_{\text{min}}}$ reduces the matching score relative to the arithmetic mean M_{mean}. The factor 1.25 is a scaling coefficient and ensures that when M_{min} and M_{mean} are equal, the penalized mean remains close to the original mean. The constants 0.25 and 1.25 were determined empirically; a lower value in place of 0.25 would decrease the penalty for low minimum scores. This approach ensures that extremely low minimum values – indicating a clearly unmet criterion – have a stronger influence on the matching score since we expect a contrail to match all criteria reasonably well to match the flight. This strategy is also applied because the individual score ranges have been defined generously in order to account for uncertainties in the calculation of contrail life cycle properties (e.g., contrail formation time and position). We adopt more permissive score ranges and avoid overly strict evaluation of any single criterion but eventually we weight lower scores more heavily to reflect the reduced confidence associated with poorly satisfied criteria. The matching score does not represent a probability. $M = 0$ means insufficient consistency with the flight. The higher the value of M, the greater the consistency of the cluster with the flight. Clusters that receive $M > 0$ are referred to as matches in the following. Thresholds $M > 0.4 - 0.5$ can be used to capture robust matches. A lower threshold can be applied if the goal is to maximize recall by including all potential candidates, whereas a higher threshold can be used to ensure high precision by restricting the selection to instances where the attribution to the flight is highly confident.

https://doi.org/10.5194/egusphere-2026-3046
Preprint. Discussion started: 28 July 2026

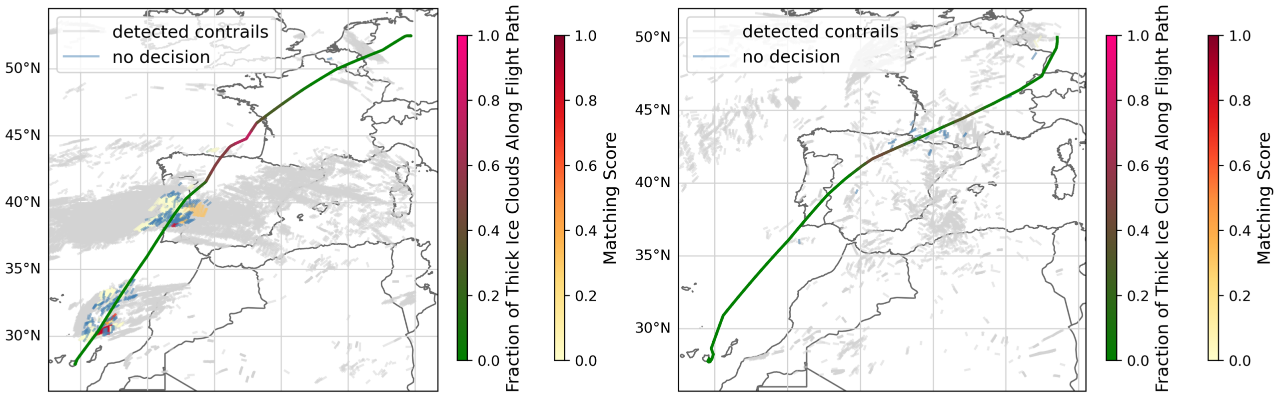

Figure 4. Matching results for two example flights on 3 May 2024 (left) and 29 August 2024 (right). All detected contrails from the start of the flight until two hours after landing are displayed.

325 ### 3.6 Application

Fig. 4 shows the matching result for one flight with contrail matches (left) and one without contrail matches (right). In the first, multiple contrail matches are identified, including three with particularly high scores ($M > 0.8$), likely generated by the flight. For the second flight, several detected contrails are near the flight track, but none fulfils $M > 0$. The flight path is colour-coded according to the fraction of flight path traversing thick ice clouds. In the displayed flights, the fraction is generally low
330 (green), indicating minimal influence on contrail detection, suggesting that it does not significantly hinder the identification of contrail formation for the displayed flights. The ability to reduce several thousand initial detections to only a few plausible contrail matches highlights a key strength of the method: it fully automatically and efficiently filters large contrail datasets containing false alarms by enforcing geometric and temporal consistency. This strong reduction capability enables contrail-to-flight association, isolating only those contrails that satisfy all physically plausible constraints.

335 The computation time of the contrail-matching algorithm on a multi-core high-performance computing (HPC) cluster with 100 GB random-access memory (RAM) depends primarily on the length of the flight and the number of contrails detected. ACTA accounts for the largest share of the computational effort. Including data loading and contrail detection, the matching process for example flights of 4 h duration exhibits an average runtime of approx. 4:30 h including output data storage. In one case with only a few contrails, the total runtime was as low as approx. 0:30 h, whereas for one flight with a large number of contrails, the
340 runtime reached approx. 17:30 h. Through batch processing, multiple flights can be evaluated simultaneously, which supports efficient large-scale analysis.

https://doi.org/10.5194/egusphere-2026-3046
Preprint. Discussion started: 28 July 2026

4 Discussion

To assess the validity and reliability of the developed algorithm, a validation of the method and a detailed analysis of potential uncertainties are performed. Significant uncertainty arises from contrail detection, influenced by the moderate spatial resolution of MSG/SEVIRI and the resulting moderate/low values of recall/precision. Furthermore, uncertainties are inherent in the derivation of the life cycle parameters and the set-up of the five scores.

4.1 Contrail Detection

Uncertainties in contrail detection affect the matching results through both false alarms and missed detections. Matching results based on automated and manual contrail detections for four flight segments (two with many contrails and two with a moderate amount of contrails) are compared. The manual contrail detection serves as an approximation of the ground truth. Manual contrail labeling is often used as a reference for contrail detection (e.g. Mannstein et al., 1999; Meijer et al., 2024; Ng et al., 2024; Santos Gabriel et al., 2026a), but it is known to bear intrinsic uncertainties due to the challenges faced by manual labelers when identifying contrails (Santos Gabriel et al., 2026a). In this study one person was assigned to each of the four segments. The manual detection was performed by visually inspecting MSG/SEVIRI Ash RGB composite imagery. For each identified contrail, the human labelers manually defined the coordinates of the contrail endpoints. After contrail detection, the matching procedure is applied to both contrail datasets.

Fig. 5 shows that the automated (first row) and manual (second row) detection identify similar but not identical contrail patterns. The automatic detection is characterised by a higher contrail density, with more shorter objects and a number of false alarms compared to the manual contrail detection (first column), but with similar patterns, i.e., a large contrail area west of the flight track, and various small contrail sequences east of it. The different contrail distributions induce different cluster building, with less but larger clusters in the human labeled contrails (second column). Despite these initial differences, both matching procedures produce the same number of contrail clusters with matching score $M > 0$. Using manual detections, four matches are obtained, three of which exhibit high matching scores $M \approx$ 0.8–1 in areas A, B and D. The automated detection also yields four matches, two of them with comparably high scores, and all of them are located in area A, the area with the highest contrail density east of the flight track. The contrail match with the highest score in area A is identical in both the automated and manual detections, the other matches do not coincide. Three matches appear exclusively in the manual detection in areas B, C, D. Further analysis using MSG/SEVIRI imagery suggests that the one in area D is optically very thin and was therefore likely missed by the automated detection. The other two manual matches in area B and C are detected automatically, but only in fewer time steps and over shorter spatial extents. Since these contrails are shorter, there are larger uncertainties in the clustering. Consequently, the match in area C is not successfully clustered (contrails exhibit strong temporal variability in length or orientation / contrails remain undetected) and is assigned a status of no decision. The match in area B receives a matching score of 0, as only a minor portion of its life cycle is captured automatically and this portion does not satisfy the matching criteria with the flight. For the three matches located in area A, which appear exclusively in the automated detection, MSG imagery suggests that they may correspond to segments of the common match of manual and automated detection in

https://doi.org/10.5194/egusphere-2026-3046
Preprint. Discussion started: 28 July 2026

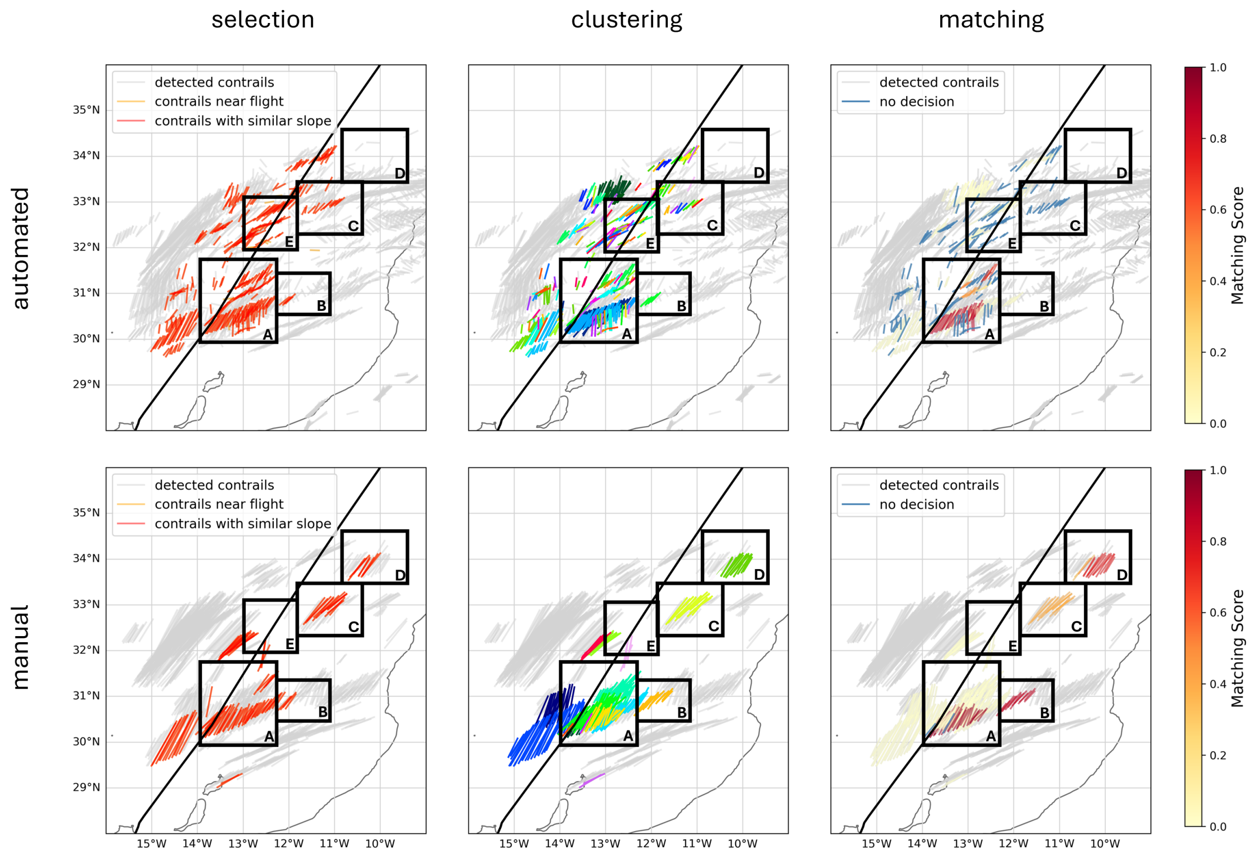

Figure 5. Intermediate steps and outcomes of the contrail-to-flight matching for a flight segment, using automated detections (top row) and manual detections (bottom row). The first column depicts all detected contrails (gray), those close to the flight path (orange), and those also exhibiting a similar slope to the flight (red). In the second column, contrails are shown after clustering, with each cluster in a distinct colour. The third column illustrates the matching results, with contrails colour-coded according to their matching score.

https://doi.org/10.5194/egusphere-2026-3046
Preprint. Discussion started: 28 July 2026

area A. However, since these segments are difficult to discern and labelling is inherently subjective, they were not included in the manual detection. Finally, area E shows various false alarms (no corresponding manual detection) that are classified as "no decision" by the matching procedure since these objects cannot be reliably tracked across multiple time steps. This has also been observed in the case of intermittent detections caused by low optical thickness.

Overall, both methods produce realistic results, each with its own uncertainties. The automated approach is efficient and consistent, while manual labelers tend to identify longer contrails and follow them consistently over their lifetime, guided by background knowledge of their expected or idealised temporal evolution. In the automated procedure, detection uncertainties may prevent detections from being correctly associated to the same cluster across time steps or may prevent the creation of a cluster at all. On the other hand, automated detections are also able to detect smaller contrails that might be missed by humans. Furthermore, when applying this matching method to evaluate contrail mitigation efforts, the occasional omission of very thin, short or short-lived contrails by the automated algorithm may be of secondary importance, as these typically contribute less to the overall radiative forcing and are thus less critical for avoidance strategies. Furthermore, the tracking mechanism – that penalises inconsistencies arising from temporal variability in contrail length or orientation – enhances the robustness of our results by filtering out false alarms, thus alleviating one of the most hindering characteristics of automated contrail detection for MSG/SEVIRI, the low precision of the algorithm. Thus, in this example both detection methods lead to plausible potential matches with high score. The remaining analysed three flight segments show similar behaviour, supporting the robustness of the findings (Appendix C).

4.2 Contrail-to-Flight Matching

By construction, the matching procedure evaluates each flight independently and does not account for surrounding air traffic. Consequently, a high matching score $M > 0$ indicates a physically plausible assignment to the target flight, but does not imply an exclusive association. In regions with high traffic density, a contrail could potentially be attributed to multiple flights operating in close spatial and temporal proximity. Accounting for the surrounding air traffic would only alter the outcome if another flight yields a higher matching score for the same contrail. For cases where the current score is zero, the matching criteria are inherently unsatisfied; accounting for additional flights would not change this result. Beyond the computational overhead, incorporating general air traffic would require access to the respective flight trajectories as well as a complex strategy to define a relevant spatio-temporal search domain. While the matching procedure could, in principle, be iteratively applied to surrounding flights for a more robust attribution, this extension would substantially increase the computational demand and remains a subject for future investigations.

The selection step is a critical component of the matching procedure, as it defines the potential candidates and establishes the foundation for all subsequent scoring and attribution. Consequently, this stage is a primary focus of our uncertainty analysis to ensure that the initial constraints do not prematurely exclude valid contrails. The parameters were chosen to be larger than what would be required based on typical wind conditions. This approach ensures that no relevant contrails are excluded; The sensitivity of the matching results to these selection parameters is evaluated by increasing both thresholds – the shell size and the allowable change in orientation – by 10 % (shell radius from 1.39 to 1.53 pixels per 5 min, orientation tolerance from 2.80°

https://doi.org/10.5194/egusphere-2026-3046
Preprint. Discussion started: 28 July 2026

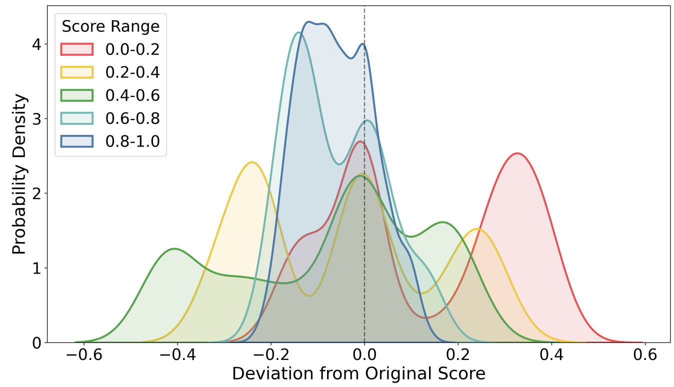

Figure 6. Sensitivity of the matching score M to perturbations in the scores M_1, M_2, M_4, and M_5. The kernel density estimate (KDE) shows the distribution of deviations from the original matching score after varying the scores by ± 0.2 in multiple combinations. The data is stratified into five score ranges.

to 3.08° per 5 min) for four flights. As expected, more contrails are initially identified, but after subsequent processing, the number of matches with a score greater than 0.5 – a threshold for ensuring a high degree of confidence in contrail attribution – remained 0 for one flight and increased from 0 to 1 for another. For the two flights with very high contrail density, the number of matches rose from 6 to 9 and from 11 to 16, respectively. These results indicate that the matching outcomes are sensitive to selection parameters primarily under high contrail density, where the contrail matching is most challenging. However, the relatively small increase in the number of matches suggests that the contrail selection is stable with respect to the underlying parameters.

In addition to the selection parameters, the sensitivity of the matching score itself to the underlying scoring criteria was investigated. The thresholds for the score criteria are empirically determined and we assess in the following how variations in the individual score components affect the matching score. For this purpose, four flights were selected: two characterized by a high number of contrail matches and two with low match counts. For every contrail cluster, the scores M_1, M_2, M_4, and M_5 were systematically varied. The direction consistency score M_3 was excluded from this variation, as it consists of a binary classifier (0 or 1) based on the correctness of the movement direction, leaving no room for continuous intermediate adjustments. The scores were perturbed both individually and in combinations of two, three, or all four simultaneously, by introducing a variation of $\pm$ 0.2. The resulting modified scores were then compared against the original scores. Fig. 6 displays the absolute deviation between the perturbed and original matching scores, categorized into five distinct score intervals (5 bins of size 0.2 from $M = 0$ to $M = 1$). The analysis reveals that higher matching scores exhibit a high degree of robustness; for the range 0.8–1.0 (dark blue), the distribution is narrow and centered near zero, with an mean absolute difference of only 0.08. As the matching scores decrease, the distributions become broader, indicating an increasing sensitivity to parameter perturbations. However, even within the lowest score interval (0.0–0.2, red), the mean absolute deviation remains bounded at 0.19, indicating that the scoring system does not suffer from excessive volatility. Furthermore, the statistical evaluation demonstrates that

https://doi.org/10.5194/egusphere-2026-3046
Preprint. Discussion started: 28 July 2026

68.3 % of the contrails maintain their status as a match ($M > 0$) throughout the perturbations. In 18.7 % of the cases, a contrail previously classified as a match shifted to $M = 0$ (no match), while in 13.0 % of the cases, a non-match ($M = 0$) was elevated to a match ($M > 0$). These findings confirm that while lower scores are inherently more sensitive to parameter definitions, the overall contrail attribution remains stable.

5 Conclusions

This study presents an automated multi-step method that enables a quantitative assessment of how well an observed contrail can be attributed to a specific flight, based on Rapid Scan data from the MSG/SEVIRI satellite sensor. The method integrates several steps – from contrail selection based on spatial proximity and alignment with the flight trajectory, through a two-stage contrail tracking process and a quantitative evaluation of how consistent a contrail's life cycle is with a given flight, represented by a matching score. This approach not only allows for contrail-to-flight attribution, but it also provides a measure of its confidence, representing an advancement over binary classification methods. Unlike methods that advect flight paths using external wind fields, this approach relies on visual contrail tracking. This eliminates a source of meteorological uncertainty and provides a fully observation-based attribution process. Applying the methodology to two case studies illustrates its robust filtering capability, as it reduces thousands of initial candidates to only a few physically consistent contrail-to-flight associations.

The method effectively overcomes the high false alarm rate typical of automatic contrail detection in MSG/SEVIRI data, addressing a major methodological challenge. Although manual detection could potentially capture more actual contrails, this approach is considerably more time consuming, subjective, and also limited by the spatial resolution of satellite data. While the current implementation focuses on individual flights, a high matching score $M > 0$ confirms a physically plausible assignment. In dense air traffic scenarios, this association remains valid even if not necessarily exclusive. Importantly, for cases with a score of zero, the lack of a match is definitive; including surrounding air traffic would not alter this outcome, as the criteria for a match are inherently unsatisfied. Thus, if anything, the algorithm can be expected to overestimate the number of contrails matched to a specific flight. The method demonstrates high potential for automated, observation-based verification of contrail mitigation strategies in practice.

While selecting flight trajectories in lower-density air traffic regions would facilitate a clearer interpretability of results, technical improvements to the algorithm itself should focus on integrating satellite data with higher spatial and temporal resolution to increase the quality of contrail detection and tracking. Specifically, this could be realized using data from the Flexible Combined Imager (FCI) aboard the Meteosat Third Generation (MTG) satellite (Durand et al., 2015), launched in December 2022 and operational since December 2024. Its higher spatial resolution (2 km for thermal channels) compared to MSG/SEVIRI allows for earlier detection and more precise identification of contrails. In addition, complementary pilot observations, ground-based camera measurements, and polar-orbiting satellites could enhance the quality of the input data additionally to geostationary satellites, although this would require elaborated combination methods and would lead to increased data processing efforts. Furthermore, the framework is inherently scalable and could be further developed for use with other geostationary satellites, such as GOES (North/South America) or Himawari (Asia-Pacific), to expand the geographic scope of the analysis.

https://doi.org/10.5194/egusphere-2026-3046
Preprint. Discussion started: 28 July 2026

While this study focuses on the development and validation of the contrail-to-flight matching methodology, an important application is demonstrated in a companion paper. There, the method is applied to a contrail avoidance flight trial over Europe to quantitatively evaluate how pre-tactical flight trajectory optimizations can reduce contrail formation in real-world operations. This application highlights the method's relevance for operational assessments of climate-optimized flight routing and for informing future aviation mitigation strategies.

Appendix A: ACTA Functionality and Modifications

To track contrails with ACTA (Vazquez-Navarro et al., 2010), an initial detection at any time is required. Unlike the original approach, which identified contrails in polar-orbiting satellite data from MODIS using the algorithm of Mannstein et al. (1999), this study directly employs MSG/SEVIRI observations and applies the detection algorithm of Santos Gabriel et al. (2026b) to ensure continuous monitoring. For contrail tracking, both the original algorithm and the present approach use MSG/SEVIRI Rapid Scan data, which provide a sufficiently high temporal resolution. Brightness temperature difference (BTD) imagery of the channels 10.8 μm and 12.0 μm is used, as it enhances contrail visibility and allows detection during nighttime. The main challenge in contrail tracking arises from changes in contrail shape and position between consecutive satellite images. ACTA addresses this behaviour by exploiting the fact that parts of the linear structure are typically preserved during ageing and that positional shifts are limited. Accordingly, contrails are represented as groups of pixels with high BTD values that are at least partially aligned and located close to the contrail position identified in the previous time step. The algorithm comprises two main steps: (i) localization of the contrail in the subsequent time slot and (ii) determination of the contrail shape through the assignment of contrail pixels. In the present study, improvements were introduced to the second step, while the first step remains unchanged. Both steps are briefly summarized below, followed by a description of the implemented modifications. A detailed description of the original algorithm is provided by Vazquez-Navarro et al. (2010).

Contrail Position In the first step of ACTA, contrail pixels are assumed to be approximately aligned along a straight line that can be described by a linear equation. Between two consecutive time steps, only small changes in the line parameters are expected. Accordingly, a linear regression is applied to pixels located in the vicinity of the contrail position from the previous time step and exhibiting high BTD values to estimate the updated line equation. The orientation of the fitted line and the correlation coefficient of the regression must satisfy criteria to ensure continuity of the tracked contrail. If the criteria are fulfilled, the line equation localizes the contrail.

Contrail Shape In the second step, the shape of the contrail is determined by assigning pixels in the vicinity of the identified line to the contrail. For this end, three masks containing different types of information are constructed and combined. The first mask defines a search region extending four pixels on each side of the line. With a total width of nine pixels, this mask captures not only pixels directly along the line but also within a surrounding area of approximately 16 to 20 km. The second mask represents edges in the BTD image and is used to delineate contrail boundaries. Edge detection is performed using the Laplacian of Gaussian operator. The third mask identifies pixels with high BTD values as potential candidates and is derived from two sub-masks. The first sub-mask selects the pixels with the highest BTD value in each row within the first mask and

https://doi.org/10.5194/egusphere-2026-3046
Preprint. Discussion started: 28 July 2026

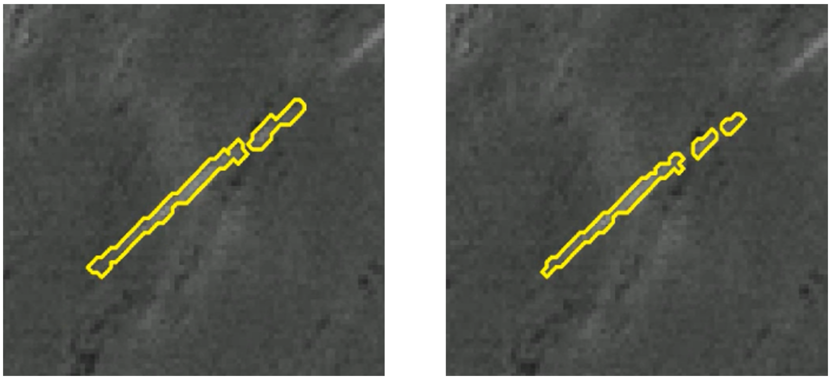

Figure A1. Contrail tracked by ACTA using different versions of the third mask. Left: original version. Right: this version.

expands them using binary dilation operator. The second sub-mask improves upon the original ACTA approach, which used a global mean BTD threshold within the first mask and often failed for low-contrast contrails. Instead, an adaptive threshold is used, whereby pixels exceeding the Gaussian-weighted local mean of their surroundings are included. The parameters of the adaptive threshold are adopted from Santos Gabriel et al. (2026b). This allows low-contrast contrails to be captured more precisely. The third mask is then obtained by multiplying the two sub-masks. The final mask is computed as the product of the three individual masks. A comparison between the final mask obtained with the original and the modified approaches is shown in Fig. A1, demonstrating the improved precision of the modified method. The parameters of the identified contrail are then used as input for the first step of the next iteration. This process is repeated until fewer than 10 pixels are detected, as the contrail becomes too diffuse to reliably determine its linear structure. Using this algorithm, contrails can be tracked over several hours in satellite imagery.

ACTA's performance is directly influenced by the contrail detection and endpoint determination, and even small variations in detected endpoints can affect its behaviour. Tracking may fail or terminate prematurely in certain cases, such as very short contrails, very low-contrast features, highly deformed or strongly non-linear structures, or in regions with many parallel or intersecting contrails.

Appendix B: Reconstruction of Contrail Formation Parameters

The contrail's potential formation location and time (i.e., where and when along the flight track) cannot be directly observed due to the delayed visibility of contrails in MSG/SEVIRI imagery. They are therefore inferred from the observed contrail life cycle, assuming homogeneous and linear motion of the contrail cluster during its early and visible lifetime. In reality, contrails are advected by upper-tropospheric winds and may follow curved trajectories.

Flight Position and Time at Contrail Formation A linear fit is applied to the sequence of contrail midpoints in the cluster.

https://doi.org/10.5194/egusphere-2026-3046
Preprint. Discussion started: 28 July 2026

The intersection of this fitted line with the flight path provides an estimate of the flight position and time where the contrail would have originated, assuming a direct causal link to the respective aircraft. Variations in contrail length during its life cycle can affect the midpoint positions, as shorter or longer contrails may shift the midpoint even if the contrail moves along a straight path.

Advection Velocity An average advection velocity is derived from the midpoints and observation times of the earliest and latest contrail in the cluster. To this end, a cluster must contain at least two contrails and the distance between the earliest and latest contrail positions shall exceed 3 pixels. This ensures that the advection velocity is not dominated by detection uncertainties or the limited spatial resolution, provides sufficient spatial variation for a meaningful assessment of advection, and avoids unreliable results from closely spaced contrails.

Advection-Derived Contrail Formation Time The advection velocity is assumed for the interval from the contrail's formation to its first detection. Using this velocity and the distance between the flight trajectory and the first detected contrail, the time at which the contrail must have been located along the trajectory is estimated.

Movement Direction The movement direction is determined based on the midpoints of the earliest and latest contrail in a cluster.

These quantities depend on the definition of the contrail endpoints. Even a one-pixel shift of the endpoints of the earliest detected contrail (corresponding to 3 km at the sub-satellite point) can have a significant impact. Assuming the contrail lies east of the flight trajectory and the endpoints of the earliest contrail are shifted by one pixel eastward, two effects occur: (i) the distance between the earliest and latest visible contrail decreases, reducing the inferred mean advection speed during the visible lifetime, and (ii) the distance to the trajectory increases. To illustrate this, we consider typical empirical values: a constant advection speed of $36\,\mathrm{km\,h^{-1}}$, a time of 0.5 h between formation and first visibility, and a visible lifetime of 1 h. Under these assumptions, the distance between the earliest and latest contrail detections is 36 km, and the distance to the flight trajectory is 18 km. A one-pixel eastward shift of the earliest detected contrail reduces the former to 33 km, lowering the inferred advection speed to $33\,\mathrm{km\,h^{-1}}$, while increasing the latter to 21 km. Combined, this results in an inferred formation time difference of more than 8 min. Assuming a cruise speed of $800\,\mathrm{km\,h^{-1}}$, an aircraft flies 107 km in that time. This is significantly larger than typical aircraft separation standards, illustrating that even sub-pixel shifts in satellite observations can lead to errors in contrail-to-flight attribution. The assumption of linear contrail motion introduces comparable uncertainties. For example, if the actual path between formation and first visibility is 20 km instead of 18 km, the advection time increases by 3.3 min, leading to a systematic underestimation of the actual advection time. Similarly, small uncertainties contrail endpoint positions affect the estimated orientation. When endpoints are separated by seven pixels, a one-pixel displacement due to detection uncertainties can change the calculated orientation by about 8°.

Appendix C: Additional Material

Figures C1, C2, and C3 provide a comparison of the matching results obtained using automated and manual contrail detections, showing consistency with the evaluation in Sect. 4.1. It should be noted that the manual labeling was restricted to the immediate

https://doi.org/10.5194/egusphere-2026-3046
Preprint. Discussion started: 28 July 2026

Table C1. Summary of scoring criteria for contrail-to-flight matching.

Score	Condition	Value
Visibility Score M_1		
Number of contrails in cluster	2	0.50
	3	0.75
	4 or more	1.00
Time Proximity Score M_2		
Time interval T between flight time	20–30 min	$\frac{T-20}{10}$
and time of first contrail observation	30–90 min	1
in minutes	90–120 min	$\frac{120-T}{30}$
	Otherwise	0
Direction Consistency Score M_3		
Movement direction	Approaching the trajectory[a]	0
	Moving away from trajectory	1
Advection Consistency Score M_4		
Temporal deviation $\|\Delta t\|$ between	< 30 min	1
estimated contrail formation time and	30–60 min	$\frac{60-\|\Delta t\|}{30}$
the flight passage time in minutes	≥ 60 min	0
Orientation Consistency Score M_5		
Comparison of angular velocities in visible and non-visible time periods[b,c]	-	$\exp\left(-\frac{\|\omega_{\text{visible}} - \omega_{\text{non visible}}\|}{\epsilon}\right)$
Matching Score M		
Combining M_1 to M_5	-	$1.25 \cdot M_{\text{mean}} \cdot \frac{M_{\text{min}}}{0.25 + M_{\text{min}}}$

[a] Or partial approach, if the earliest and latest contrail positions lie on opposite sides of the trajectory.

[b] Angular velocities are computed as $\omega_{\text{non visible}} = \frac{\Theta_0 - \Theta_1}{\Delta t_{\text{non visible}}}$, $\omega_{\text{visible}} = \frac{\Theta_1 - \Theta_2}{\Delta t_{\text{visible}}}$

[c] Decay rate $\epsilon = 0.4°$ / min (determined empirically)

https://doi.org/10.5194/egusphere-2026-3046
Preprint. Discussion started: 28 July 2026

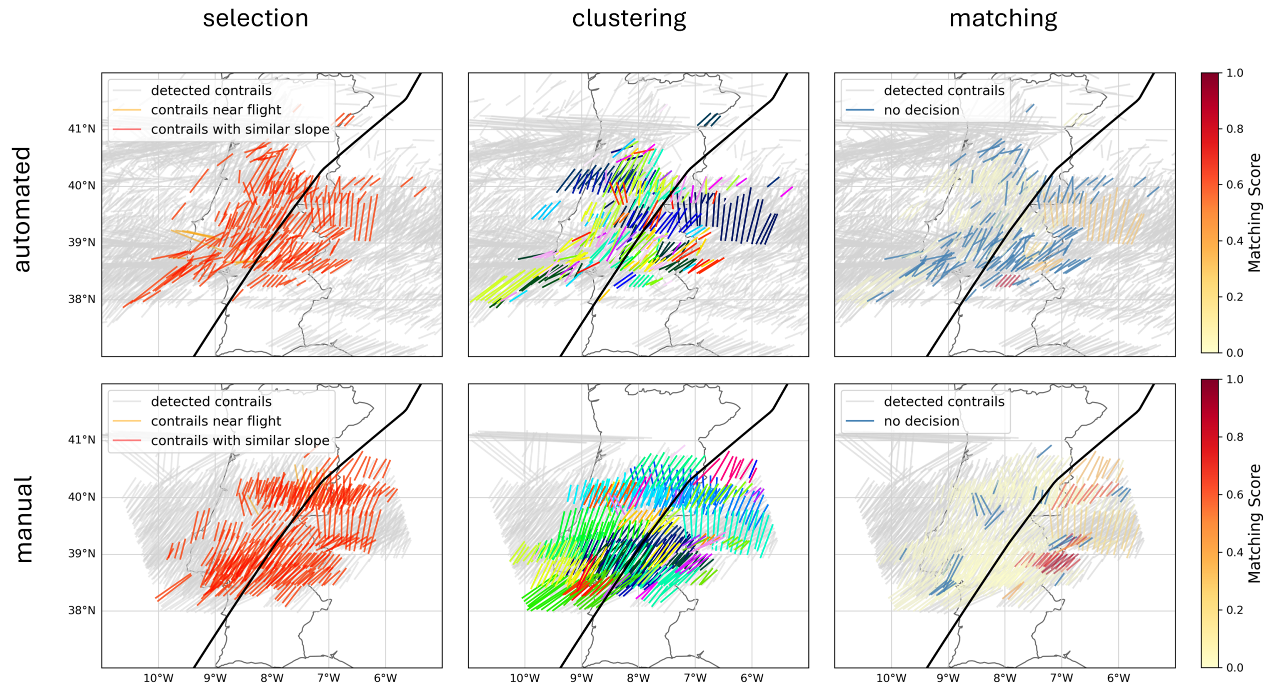

Figure C1. Intermediate steps and outcomes of the contrail–flight matching for a flight segment, using automated detections (top row) and manual detections (bottom row). The first column depicts all detected contrails (gray), those close to the flight path (orange), and those also exhibiting a similar slope to the flight (red). In the second column, contrails are shown after clustering, with each cluster in a distinct colour. The third column illustrates the matching results, with contrails colour-coded according to their matching score.

vicinity of the flight trajectories rather than the entire domain shown. Notably, the figures demonstrate that contrails with a "no decision" status are not exclusive to the automated method but also occur frequently within the manual detection framework. Interestingly, in Fig. C3 the automated algorithm identifies contrails along the flight trajectories that are entirely absent in the manual detection.

https://doi.org/10.5194/egusphere-2026-3046
Preprint. Discussion started: 28 July 2026

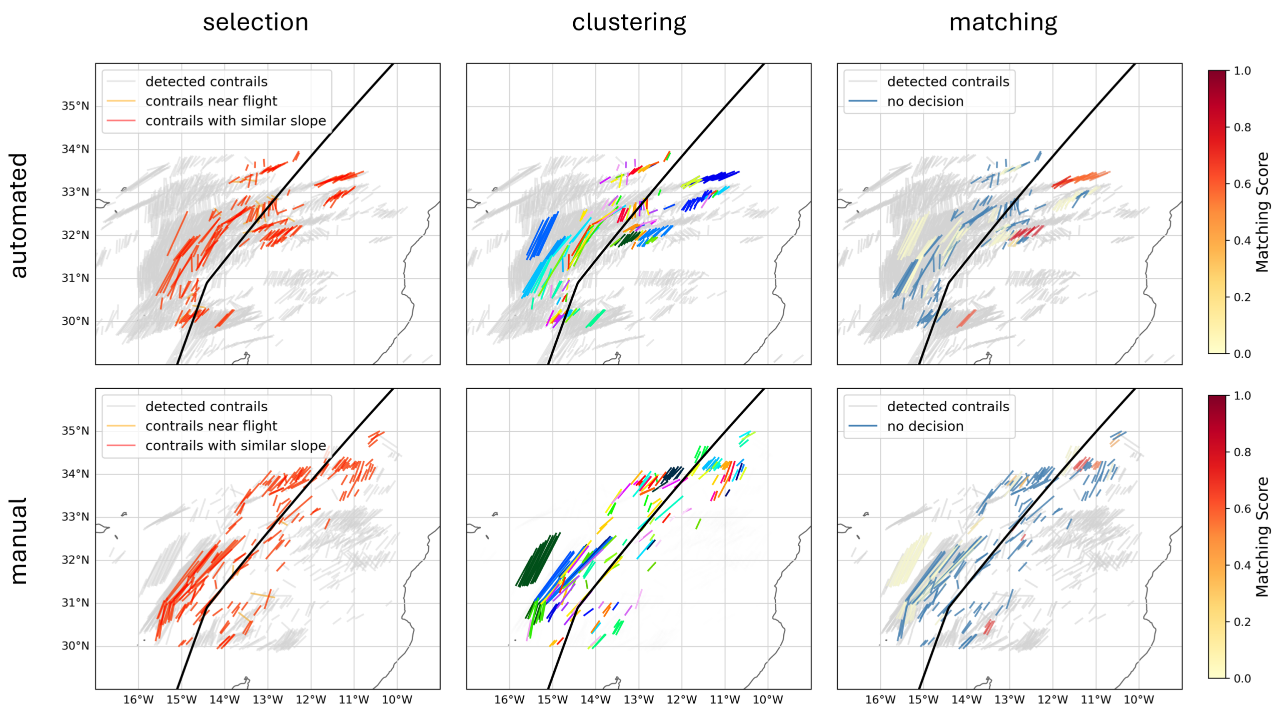

Figure C2. Intermediate steps and outcomes of the contrail–flight matching for a flight segment, using automated detections (top row) and manual detections (bottom row). The first column depicts all detected contrails (gray), those close to the flight path (orange), and those also exhibiting a similar slope to the flight (red). In the second column, contrails are shown after clustering, with each cluster in a distinct colour. The third column illustrates the matching results, with contrails colour-coded according to their matching score.

https://doi.org/10.5194/egusphere-2026-3046
Preprint. Discussion started: 28 July 2026

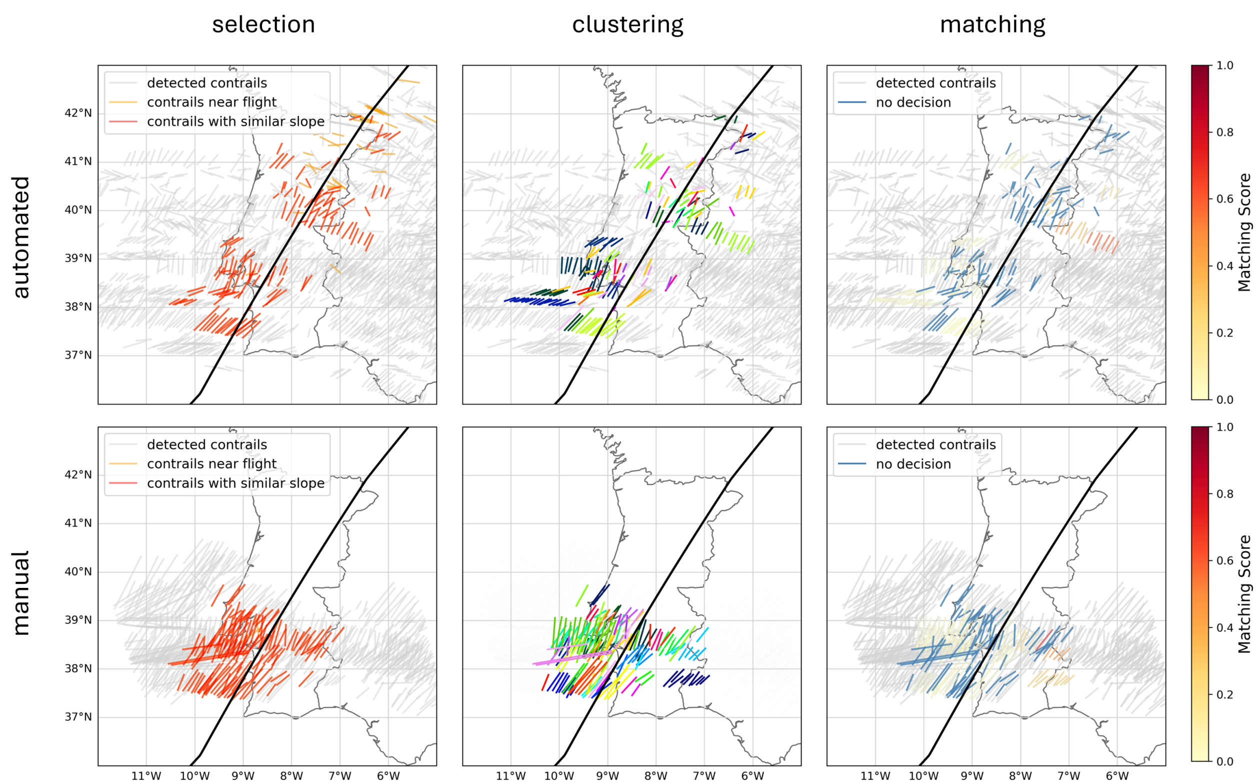

Figure C3. Intermediate steps and outcomes of the contrail–flight matching for a flight segment, using automated detections (top row) and manual detections (bottom row). The first column depicts all detected contrails (gray), those close to the flight path (orange), and those also exhibiting a similar slope to the flight (red). In the second column, contrails are shown after clustering, with each cluster in a distinct colour. The third column illustrates the matching results, with contrails colour-coded according to their matching score.

https://doi.org/10.5194/egusphere-2026-3046
Preprint. Discussion started: 28 July 2026

Data availability. Contains modified EUMETSAT Meteosat data (2025). MSG/SEVIRI data are available from the EUMETSAT (European Organisation for the Exploitation of Meteorological Satellites) data centre (https://user.eumetsat.int/catalogue/EO:EUM:DAT:MSG:HRSEVIRI, EUMETSAT, 2025).

Author contributions. SR and LB conceived this study. SR developed the presented methods with valuable feedback from LB, DP and CV. SR, LB, and VSG performed the manual labelling of contrails. DP and MA contributed to software development. MA provided a manual contrail detection tool. CV supervised the project and provided scientific advise. SR wrote the paper with the support of LB and all authors commented on the manuscript.

Competing interests. The authors declare that none of them has any competing interests.

Acknowledgements. The authors gratefully acknowledge the computational and data resources provided through the joint high-performance data analytics (HPDA) project "terrabyte" of the German Aerospace Center (DLR) and the Leibniz Supercomputing Center (LRZ). We thank TUIfly for providing flight tracks. LB acknowledges funding by the DLR Aeronautics Research Programme within the project KON-SAT. The authors thank Marie Koegstadt for her support in the manual labeling of the contrail data presented in Fig. C2. Finally, SR and LB thank Margarita Vázquez-Navarro for support in understanding ACTA.

https://doi.org/10.5194/egusphere-2026-3046
Preprint. Discussion started: 28 July 2026

References

ATAG: Waypoint 2050: An Air Transport Action Group Project, https://aviationbenefits.org/media/167417/w2050_v2021_27sept_full.pdf, accessed on July 3, 2025, 2021.

Bier, A., Unterstrasser, S., Zink, J., Hillenbrand, D., Jurkat-Witschas, T., and Lottermoser, A.: Contrail formation on ambient aerosol particles for aircraft with hydrogen combustion: a box model trajectory study, Atmos. Chem. Phys., 24, 2319–2344, https://doi.org/10.5194/acp-24-2319-2024, 2024.

Bonhorst, G., Maizet, M., and Gierens, K.: On contrail prediction under realistic weather forecast uncertainty using the example of WAWFOR data, Meteorol. Z., https://doi.org/10.1127/metz/1251, 2025.

Burkhardt, U. and Kärcher, B.: Global radiative forcing from contrail cirrus, Nat. Clim. Change, 1, 54–58, https://doi.org/10.1038/nclimate1068, 2011.

Chevallier, R., Shapiro, M., Engberg, Z., Soler, M., and Delahaye, D.: Linear Contrails Detection, Tracking and Matching with Aircraft Using Geostationary Satellite and Air Traffic Data, Aerospace, 10, https://doi.org/10.3390/aerospace10070578, 2023.

Dean, T. R., Abbott, T. H., Engberg, Z., Masson, N., Teoh, R., Itcovitz, J. P., Stettler, M. E. J., and Shapiro, M. L.: Impact of forecast stability on navigational contrail avoidance, Environ. Res.: Infrastruct. Sustain., 5, 045 008, https://doi.org/10.1088/2634-4505/ae1da5, 2025.

Driver, O. G. A., Stettler, M. E. J., and Gryspeerdt, E.: Factors limiting contrail detection in satellite imagery, Atmos. Meas. Tech., 18, 1115–1134, https://doi.org/10.5194/amt-18-1115-2025, 2025.

Duda, D. P., Minnis, P., Nguyen, L., and Palikonda, R.: A Case Study of the Development of Contrail Clusters over the Great Lakes, J. Atmos. Sci., 61, 1132 – 1146, https://doi.org/10.1175/1520-0469(2004)061<1132:ACSOTD>2.0.CO;2, 2004.

Durand, Y., Hallibert, P., Wilson, M., Lekouara, M., Grabarnik, S., Aminou, D., Blythe, P., Napierala, B., Canaud, J.-L., Pigouche, O., Ouaknine, J., and Verez, B.: The flexible combined imager onboard MTG: from design to calibration, p. 963903, https://doi.org/10.1117/12.2196644, 2015.

EUMeTrain: Compilation of RGB Recipes, https://www.eumetrain.org/sites/default/files/2022-10/RGB_recipes.pdf, accessed: 2026-02-25, 2022.

EUMETSAT: SEVIRI Rapid-Scan Service Fundamental Climate Data Record Release 1 – Product User Guide (D4.1), Product user guide, ECMWF Copernicus Climate Change Service, https://doi.org/10.15770/EUM_SEC_CLM_0098, 2024.

Geraedts, S., Brand, E., Dean, T. R., Eastham, S., Elkin, C., Engberg, Z., Hager, U., Langmore, I., McCloskey, K., Yue-Hei Ng, J., Platt, J. C., Sankar, T., Sarna, A., Shapiro, M., and Goyal, N.: A scalable system to measure contrail formation on a per-flight basis, Environ. Res. Commun., 6, 015 008, https://doi.org/10.1088/2515-7620/ad11ab, 2024.

Gettelman, A., Chen, C.-C., and Bardeen, C. G.: The climate impact of COVID-19-induced contrail changes, Atmos. Chem. Phys., 21, 9405–9416, https://doi.org/10.5194/acp-21-9405-2021, 2021.

Gierens, K. and Vazquez-Navarro, M.: Statistical analysis of contrail lifetimes from a satellite perspective, Meteorol. Z., 27, 183–193, https://doi.org/10.1127/metz/2018/0888, 2018.

Gierens, K., Matthes, S., and Rohs, S.: How Well Can Persistent Contrails Be Predicted?, Aerospace, 7, https://doi.org/10.3390/aerospace7120169, 2020.

Grewe, V., Matthes, S., Frömming, C., Brinkop, S., Jöckel, P., Gierens, K., Champougny, T., Fuglestvedt, J., Haslerud, A., Irvine, E., and Shine, K.: Feasibility of climate-optimized air traffic routing for trans-Atlantic flights, Environ. Res. Lett., 12, 034 003, https://doi.org/10.1088/1748-9326/aa5ba0, 2017.

Gryspeerdt, E., Stettler, M. E. J., Teoh, R., Burkhardt, U., Delovski, T., Driver, O. G. A., and Painemal, D.: Operational differences lead to longer lifetimes of satellite detectable contrails from more fuel efficient aircraft, Environ. Res. Lett., 19, 084 059, https://doi.org/10.1088/1748-9326/ad5b78, 2024.

Kaluza, T., Kunkel, D., and Hoor, P.: On the occurrence of strong vertical wind shear in the tropopause region: a 10-year ERA5 northern hemispheric study, Weather Clim. Dynam., 2, 631–651, https://doi.org/10.5194/wcd-2-631-2021, 2021.

Kirschler, S., Voigt, C., Piontek, D., et al.: Towards climate compatible aviation: operational feasibility of contrail avoidance by flight path adjustments, Research Square, https://doi.org/10.21203/rs.3.rs-8799231/v1, 2026.

Lee, D., Fahey, D., Skowron, A., Allen, M., Burkhardt, U., Chen, Q., Doherty, S., Freeman, S., Forster, P., Fuglestvedt, J., Gettelman, A., De León, R., Lim, L., Lund, M., Millar, R., Owen, B., Penner, J., Pitari, G., Prather, M., Sausen, R., and Wilcox, L.: The contribution of global aviation to anthropogenic climate forcing for 2000 to 2018, Atmos. Environ., 244, 117 834, https://doi.org/10.1016/j.atmosenv.2020.117834, 2021.

Li, Y., Mahnke, C., Rohs, S., Bundke, U., Spelten, N., Dekoutsidis, G., Groß, S., Voigt, C., Schumann, U., Petzold, A., and Krämer, M.: Upper-tropospheric slightly ice-subsaturated regions: frequency of occurrence and statistical evidence for the appearance of contrail cirrus, Atmos. Chem. Phys., 23, 2251–2271, https://doi.org/10.5194/acp-23-2251-2023, 2023.

Lottermoser, A. and Unterstrasser, S.: High-resolution modeling of early contrail evolution from hydrogen-powered aircraft, Atmos. Chem. Phys., 25, 7903–7924, https://doi.org/10.5194/acp-25-7903-2025, 2025.

Lottermoser, A. and Unterstrasser, S.: Modeling the Impact of Alternative Fuels and Hydrogen Propulsion on Contrail-Cirrus: A Parameter Study, J. Geophys. Res. Atmos., 131, https://doi.org/10.1029/2025JD044604, 2026.

Mannstein, H., Meyer, R., and Wendling, P.: Operational detection of contrails from NOAA-AVHRR-data, Int. J. Remote Sens., 20, 1641–1660, https://doi.org/10.1080/014311699212650, 1999.

Mannstein, H., Spichtinger, P., and Gierens, K.: A note on how to avoid contrail cirrus, Transp. Res. Part D: Transp. Environ., 10, 421–426, https://doi.org/10.1016/j.trd.2005.04.012, 2005.

Märkl, R. S., Voigt, C., Sauer, D., Dischl, R. K., Kaufmann, S., Harlaß, T., Hahn, V., Roiger, A., Weiß-Rehm, C., Burkhardt, U., Schumann, U., Marsing, A., Scheibe, M., Dörnbrack, A., Renard, C., Gauthier, M., Swann, P., Madden, P., Luff, D., Sallinen, R., Schripp, T., and Le Clercq, P.: Powering aircraft with 100 % sustainable aviation fuel reduces ice crystals in contrails, Atmos. Chem. Phys., 24, 3813–3837, https://doi.org/10.5194/acp-24-3813-2024, 2024.

Martin Frias, A., Shapiro, M. L., Engberg, Z., Zopp, R., Soler, M., and Stettler, M. E. J.: Feasibility of contrail avoidance in a commercial flight planning system: an operational analysis, Environ. Res.: Infrastruct. Sustain., 4, 015 013, https://doi.org/10.1088/2634-4505/ad310c, 2024.

Mayer, J., Mayer, B., Bugliaro, L., Meerkötter, R., and Voigt, C.: How well can brightness temperature differences of spaceborne imagers help to detect cloud phase? A sensitivity analysis regarding cloud phase and related cloud properties, Atmos. Meas. Tech., 17, 5161–5185, https://doi.org/10.5194/amt-17-5161-2024, 2024.

Meerkötter, R., Schumann, U., Doelling, D. R., Minnis, P., Nakajima, T., and Tsushima, Y.: Radiative forcing by contrails, Ann. Geophys., 17, 1080–1094, https://doi.org/10.1007/s00585-999-1080-7, 1999.

Meijer, V. R., Eastham, S. D., Waitz, I. A., and Barrett, S. R. H.: Contrail altitude estimation using GOES-16 ABI data and deep learning, Atmos. Meas. Tech., 17, 6145–6162, https://doi.org/10.5194/amt-17-6145-2024, 2024.

Myhre, G. and Stordal, F.: On the tradeoff of the solar and thermal infrared radiative impact of contrails, Geophys. Res. Lett., 28, 3119–3122, https://doi.org/https://doi.org/10.1029/2001GL013193, 2001.

https://doi.org/10.5194/egusphere-2026-3046
Preprint. Discussion started: 28 July 2026

Ng, J. Y.-H., McCloskey, K., Cui, J., Meijer, V. R., Brand, E., Sarna, A., Goyal, N., Van Arsdale, C., and Geraedts, S.: Contrail Detection on GOES-16 ABI With the OpenContrails Dataset, IEEE Trans. Geosci. Remote Sens., 62, 1–14, https://doi.org/10.1109/TGRS.2023.3345226, 2024.

Petzold, A., Neis, P., Rütimann, M., Rohs, S., Berkes, F., Smit, H. G. J., Krämer, M., Spelten, N., Spichtinger, P., Nédélec, P., and Wahner, A.: Ice-supersaturated air masses in the northern mid-latitudes from regular in situ observations by passenger aircraft: vertical distribution, seasonality and tropospheric fingerprint, Atmos. Chem. Phys., 20, 8157–8179, https://doi.org/10.5194/acp-20-8157-2020, 2020.

Prather, M. J., Gettelman, A., and Penner, J. E.: Trade-offs in aviation impacts on climate favour non-CO2 mitigation, Nature, 643, 988–993, https://doi.org/10.1038/s41586-025-09198-2, 2025.

Santos Gabriel, V., Bugliaro, L., Montag, M., Ries, S., Wang, Z., Widmaier, K., Arico, M., Unterstrasser, S., Mayer, J., Menekay, D., Marsing, A., de la Torre Castro, E., Megill, L., Scheibe, M., and Voigt, C.: A manually labeled contrail dataset from MSG/SEVIRI, Earth Syst. Sci. Data, 18, 2397–2412, https://doi.org/10.5194/essd-18-2397-2026, 2026a.

Santos Gabriel, V., Bugliaro, L., Piontek, D., Ries, S., and Voigt, C.: An adaptive segmentation approach for contrail detection in meteosat second generation satellite imagery, Atmos. Meas. Tech., 19, 3271–3289, https://doi.org/10.5194/amt-19-3271-2026, 2026b.

Sarna, A., Meijer, V., Chevallier, R., Duncan, A., McConnaughay, K., Geraedts, S., and McCloskey, K.: Benchmarking and improving algorithms for attributing satellite-observed contrails to flights, Atmos. Meas. Tech., 18, 3495–3532, https://doi.org/10.5194/amt-18-3495-2025, 2025.

Sausen, R., Hofer, S., Gierens, K., Bugliaro, L., Ehrmanntraut, R., Sitova, I., Walczak, K., Burridge-Diesing, A., Bowman, M., and Miller, N.: Can we successfully avoid persistent contrails by small altitude adjustments of flights in the real world?, Meteorol. Z., 33, 83–98, https://doi.org/10.1127/metz/2023/1157, 2024.

Schmetz, J., Pili, P., Tjemkes, S., Just, D., Kerkmann, J., Rota, S., and Ratier, A.: AN INTRODUCTION TO METEOSAT SECOND GENERATION (MSG), Bull. Am. Meteorol. Soc., 83, 977 – 992, https://doi.org/10.1175/1520-0477(2002)083<0977:AITMSG>2.3.CO;2, 2002.

Schmit, T. J., Griffith, P., Gunshor, M. M., Daniels, J. M., Goodman, S. J., and Lebair, W. J.: A Closer Look at the ABI on the GOES-R Series, Bull. Am. Meteorol. Soc., 98, 681 – 698, https://doi.org/10.1175/BAMS-D-15-00230.1, 2017.

Schumann, U.: A contrail cirrus prediction model, Geosci. Model Dev., 5, 543–580, https://doi.org/10.5194/gmd-5-543-2012, 2012.

Schumann, U., Hempel, R., Flentje, H., Garhammer, M., Graf, K., Kox, S., Lösslein, H., and Mayer, B.: Contrail study with ground-based cameras, Atmos. Meas. Tech., 6, 3597–3612, https://doi.org/10.5194/amt-6-3597-2013, 2013.

Schumann, U., Poll, I., Teoh, R., Koelle, R., Spinielli, E., Molloy, J., Koudis, G. S., Baumann, R., Bugliaro, L., Stettler, M., and Voigt, C.: Air traffic and contrail changes over Europe during COVID-19: a model study, Atmos. Chem. Phys., 21, 7429–7450, https://doi.org/10.5194/acp-21-7429-2021, 2021.

Seelig, T., Wolf, K., Bellouin, N., and Tesche, M.: Quantification of the radiative forcing of contrails embedded in cirrus clouds, Nature Commun., 16, 10 703, https://doi.org/10.1038/s41467-025-66231-8, 2025.

Simmons, A. J.: Trends in the tropospheric general circulation from 1979 to 2022, Weather Clim. Dyn., 3, 777–809, https://doi.org/10.5194/wcd-3-777-2022, 2022.

Smith, J. R., Grobler, C., Hodgson, P. J., Mukhopadhaya, J., Shapiro, M. L., Mirolo, M., Stettler, M. E. J., Eastham, S. D., and Barrett, S. R. H.: The climate opportunities and risks of contrail avoidance, Nature Commun., 17, 2092, https://doi.org/10.1038/s41467-026-68784-8, 2026.

https://doi.org/10.5194/egusphere-2026-3046
Preprint. Discussion started: 28 July 2026

Sonabend-W, A., Elkin, C., Dean, T., et al.: Feasibility test of per-flight contrail avoidance in commercial aviation, Commun Eng, 3, 184, https://doi.org/10.1038/s44172-024-00329-7, 2024.

Strandgren, J., Bugliaro, L., Sehnke, F., and Schröder, L.: Cirrus cloud retrieval with MSG/SEVIRI using artificial neural networks, Atmos. Meas. Tech., 10, 3547–3573, https://doi.org/10.5194/amt-10-3547-2017, 2017.

Teoh, R., Schumann, U., Majumdar, A., and Stettler, M. E. J.: Mitigating the Climate Forcing of Aircraft Contrails by Small-Scale Diversions and Technology Adoption, Environ. Sci. Technol., 54, 2941–2950, https://doi.org/10.1021/acs.est.9b05608, 2020a.

Teoh, R., Schumann, U., and Stettler, M. E. J.: Beyond Contrail Avoidance: Efficacy of Flight Altitude Changes to Minimise Contrail Climate Forcing, Aerospace, 7, https://doi.org/10.3390/aerospace7090121, 2020b.

Teoh, R., Schumann, U., Gryspeerdt, E., Shapiro, M., Molloy, J., Koudis, G., Voigt, C., and Stettler, M. E. J.: Aviation contrail climate effects in the North Atlantic from 2016 to 2021, Atmos. Chem. Phys., 22, 10 919–10 935, https://doi.org/10.5194/acp-22-10919-2022, 2022a.

Teoh, R., Schumann, U., Voigt, C., Schripp, T., Shapiro, M., Engberg, Z., Molloy, J., Koudis, G., and Stettler, M. E. J.: Targeted Use of Sustainable Aviation Fuel to Maximize Climate Benefits, Environ. Sci. Technol., 56, 17 246–17 255, https://doi.org/10.1021/acs.est.2c05781, 2022b.

Teoh, R., Engberg, Z., Schumann, U., Voigt, C., Shapiro, M., Rohs, S., and Stettler, M. E. J.: Global aviation contrail climate effects from 2019 to 2021, Atmos. Chem. Phys., 24, 6071–6093, https://doi.org/10.5194/acp-24-6071-2024, 2024.

Vazquez-Navarro, M., Mannstein, H., and Mayer, B.: An automatic contrail tracking algorithm, Atmos. Meas. Tech., 3, 1089–1101, https://doi.org/10.5194/amt-3-1089-2010, 2010.

Vázquez-Navarro, M., Mannstein, H., and Kox, S.: Contrail life cycle and properties from 1 year of MSG/SEVIRI rapid-scan images, Atmos. Chem. Phys., 15, 8739–8749, https://doi.org/10.5194/acp-15-8739-2015, 2015.

Voigt, C.: Solving aviation's climate-action conundrum, Nature, 643, 921–923, https://doi.org/10.1038/d41586-025-02129-1, 2025.

Voigt, C., Kleine, J., Sauer, D., et al.: Cleaner burning aviation fuels can reduce contrail cloudiness, Commun. Earth Environ., 2, 114, https://doi.org/10.1038/s43247-021-00174-y, 2021.

Voigt, C., Märkl, R., Sauer, D., Dischl, R., Renard, C., Seeliger, K., Yu, F., Kaufmann, S., Bräuer, T., Jurkat-Witschas, T., Le Chenadec, G., Moreau, J., Requena-Esteban, E., Bonne, N., Vals, M., Roche, A., Zelina, J., Dörnbrack, A., Eirenschmalz, L., Heckl, C., Horst, E., Lichtenstern, M., Marsing, A., Neumann, G., Roiger, A., Scheibe, M., Stock, P., Giez, A., Eckel, G., and Le Clercq, P.: Substantial aircraft contrail formation at low soot emission levels, Nature, 652, 112–118, https://doi.org/10.1038/s41586-026-10286-0, 2026.

Wang, Z. and Voigt, C.: Tracing contrails within cirrus clouds and their climate effect, Nature Commun., 16, 10 702, https://doi.org/10.1038/s41467-025-66724-6, 2025.

Winker, D. M., Vaughan, M. A., Omar, A., Hu, Y., Powell, K. A., Liu, Z., Hunt, W. H., and Young, S. A.: Overview of the CALIPSO Mission and CALIOP Data Processing Algorithms, J. Atmos. Ocean. Technol., 26, 2310 – 2323, https://doi.org/10.1175/2009JTECHA1281.1, 2009.

Wu, L., Su, H., Zeng, X., Posselt, D. J., Wong, S., Chen, S., and Stoffelen, A.: Uncertainty of Atmospheric Winds in Three Widely Used Global Reanalysis Datasets, J. Appl. Meteorol. Climatol., 63, 165 – 180, https://doi.org/10.1175/JAMC-D-22-0198.1, 2024.